Received: 9 November 2022 | Revised: 5 April 2023 | Accepted: 8 April 2023

DOI: 10.1111/gcb.16762

Global Change Biology WILEY

RESEARCH ARTICLE

The North American Monsoon buffers forests against the ongoing megadrought in the Southwestern United States

Brandon M. Strange[1,2] | Russell K. Monson[2,3] | Paul Szejner[2,4] | Jim Ehleringer[5] | Jia Hu[1,2]

[1]School of Natural Resources and the Environment, University of Arizona, Tucson, Arizona, USA

[2]Laboratory of Tree Ring Research, University of Arizona, Tucson, Arizona, USA

[3]Department of Ecology and Evolutionary Biology, University of Arizona, Tucson, Arizona, USA

[4]Instituto de Geología, Universidad Nacional Autónoma de México, México City, Mexico

[5]School of Biological Sciences, University of Utah, Salt Lake City, Utah, USA

Correspondence
Brandon M. Strange, School of Natural Resources and the Environment, University of Arizona, Tucson, AZ, USA.
Email: bstrange@arizona.edu

Funding information
National Science Foundation, Grant/Award Number: 1065790 and 1754430

Abstract

The US Southwest has been entrenched in a two-decade-long megadrought (MD), the most severe since 800 CE, which threatens the long-term vitality and persistence of regional montane forests. Here, we report that in the face of record low winter precipitation and increasing atmospheric aridity, seasonal activity of the North American Monsoon (NAM) climate system brings sufficient precipitation during the height of the summer to alleviate extreme tree water stress. We studied seasonally resolved, tree-ring stable carbon isotope ratios across a 57-year time series (1960–2017) in 17 Ponderosa pine forests distributed across the NAM geographic domain. Our study focused on the isotope dynamics of latewood (LW), which is produced in association with NAM rains. During the MD, populations growing within the core region of the NAM operated at lower intrinsic and higher evaporative water-use efficiencies (WUE_i and WUE_E, respectively), compared to populations growing in the periphery of the NAM domain, indicating less physiological water stress in those populations with access to NAM moisture. The disparities in water-use efficiencies in periphery populations are due to a higher atmospheric vapor pressure deficit (VPD) and reduced access to summer soil moisture. The buffering advantage of the NAM, however, is weakening. We observed that since the MD, the relationship between WUE_i and WUE_E in forests within the core NAM domain is shifting toward a drought response similar to forests on the periphery of the NAM. After correcting for past increases in the atmospheric CO_2 concentration, we were able to isolate the LW time-series responses to climate alone. This showed that the shift in the relation between WUE_i and WUE_E was driven by the extreme increases in MD-associated VPD, with little advantageous influence on stomatal conductance from increases in atmospheric CO_2 concentration.

KEYWORDS
ecophysiology, megadrought, North American Monsoon, stable isotopes, tree rings, water-use efficiency

1 | INTRODUCTION

Since ~2000 CE an extreme "megadrought" (MD), defined by two continuous decades of anomalously low precipitation and elevated temperatures (Szejner et al., 2020, 2021; Williams et al., 2020), has persisted in the Southwestern United States (SWUS). One recent study estimated the current MD to be the most severe drought in this region since at least 800 CE (Williams et al., 2022), with the cause being attributed to progressive anthropogenic climate change (Williams et al., 2020). The MD has caused decreases in regional

snowpack and shifts toward earlier melt dates (Mote et al., 2018; Musselman et al., 2021), affecting montane forests that rely on winter precipitation for growth (Szejner et al., 2020). In some regions, extreme summer temperature maxima during the MD have amplified the effects of forest drought stress and increased tree mortality (Allen et al., 2010; Breshears et al., 2005; Ganey & Vojta, 2011; Williams et al., 2013). In general, the pattern of forest response to the MD has been highly variable, depending on location, and influenced by regional climate gradients (Szejner et al., 2021). In certain forests, the North American Monsoon (NAM) climate system, which can deliver up to 60% of the annual precipitation from July to September (Sheppard et al., 2002), has interrupted summertime drought extremes and potentially provided a reprieve from MD stress. The degree to which this has occurred, however, is uncertain given the unprecedented length and severity of the current drought. In this study, we addressed this uncertainty by asking the question: to what extent have NAM rains buffered forests against the extreme conditions of the MD across its entire two-decade span?

Chronologies of tree-ring widths have been used in several past studies of forest responses to climate in the SWUS, with an explicit aim to examine the influence of the NAM on forest productivity (Griffin et al., 2013; Kerhoulas et al., 2017; Peltier & Ogle, 2019; Yocom et al., 2022). Our aim was to develop a more focused physiological metric by which to explore these responses. We constructed long-term time series of seasonally resolved ring width and stable carbon isotopes for 17 forests distributed across the core and periphery of the NAM domain. We focused on ponderosa pine (*Pinus ponderosa*) forests, which comprise a large percentage of montane ecosystems in the SWUS. Montane ponderosa pine forests play a major role in the carbon budget of the Western United States (Schimel et al., 2002) and determine many of the regional snow hydrology dynamics (O'Donnell et al., 2021). To examine physiological responses to NAM moisture, we used estimates of intrinsic water-use efficiency (WUE_i), derived from latewood (LW) carbon isotopic ratios ($^{13}C/^{12}C$) of tree-ring cellulose. WUE_i reflects the ratio of net CO_2 assimilation rate (A) to stomatal conductance (g_s; Farquhar et al., 1989), and has been shown to be sensitive to atmospheric CO_2 concentrations (c_a), vapor pressure deficit (VPD), and soil moisture deficit (Andreu-Hayles et al., 2011; Francey & Farquhar, 1982; Kannenberg et al., 2021; Saurer et al., 2004).

WUE_i has increased globally over the past century along with c_a (Adams et al., 2020; Mathias & Thomas, 2021), and both decreases in g_s or increases in A can explain past trends in WUE_i, depending on region and forest type (Adams et al., 2020; Guerrieri et al., 2019; Lavergne et al., 2019; Mathias & Thomas, 2021). An additional complication is that reductions in g_s can be caused by increases in c_a (Ainsworth & Rogers, 2007) or VPD (Grossiord et al., 2020), or both, thus complicating insight into underlying causes. Even if the influences of c_a and VPD on WUE_i are resolved, however, there is uncertainty about how well WUE_i represents the true water use of a tree, since the water-to-carbon tradeoff is ultimately determined by transpiration rate (E), not g_s. While independent observations of WUE_i provide insight into intrinsic controls over A and g_s, they only reflect accurate patterns in E if they are evaluated at constant VPD or if the effects of VPD on E are explicitly considered (Franks et al., 2013).

In semi-arid regions of the western United States. where aridity (VPD) has steadily increased, it is becoming increasingly clear that WUE_i is not the best metric to represent any potential water savings through reductions in g_s. Because of these challenges, we evaluated forest responses to the MD by employing not only WUE_i but also evaporative water-use efficiency ($WUE_E = A/(g_s \times VPD)$; or A/E). Although WUE_E is commonly referred to as instantaneous water-use efficiency (Farquhar & Richards, 1984; Seibt et al., 2008), we refer to it here as evaporative water-use efficiency, as it is used to evaluate the response of E to increased aridity. By combining the two WUE metrics, we accounted for both the indirect (through g_s) and direct (through E) responses of trees to increases in VPD. Our primary aim was to examine the importance of the NAM in insulating forests from drought stress during the current MD. Additionally, we addressed two secondary objectives using the dual WUE approach: (1) to isolate the direct and indirect responses of WUE to VPD, and (2) to examine the potential for increased VPD during the MD to enhance or mitigate the CO_2 sensitivity of WUE_i and WUE_E.

2 | MATERIALS AND METHODS

2.1 | Study area

The study was conducted at 17 forested sites spanning the geographic area between latitudes 32.41°N to 39.36°N and longitudes 105.77°W to 113.47°W (Figure 1). Montane forests in this area are dominated by *P. ponderosa* subspecies *brachyptera* Engelm. The study sites occur across a gradient of NAM precipitation where some sites reliably receive summertime moisture from the NAM (referred to here as the NAM-core), while others receive less precipitation from the NAM (referred to as the NAM-periphery). Detailed maps of the sites in relation to gradients in seasonal precipitation and atmospheric VPD are shown in Figure 1.

2.2 | Sample collection and preparation

At each study site, 57-year chronologies, beginning in 1960, were constructed of LW ring width index and $^{13}C/^{12}C$ carbon isotope ratios of extracted LW cellulose. We collected two cores at breast height from 10 to 20 trees at each site using 12 or 5 mm increment borers. Trees were selected on the following criteria: canopy dominant, no apparent fire disturbances or forest management practices, no apparent disease or dieback, and approximately 100–250 years old to ensure adequately sized rings for isotope analysis.

Each core was sanded with fine-grain sandpaper, scanned and statistically cross-dated using COFECHA (Holmes, 1983). Annually dated rings were subdivided into three sections: the earlywood portion of the ring was divided into two halves (EW1 and EW2), while the LW portion of the ring was its own section (LW). Each of the

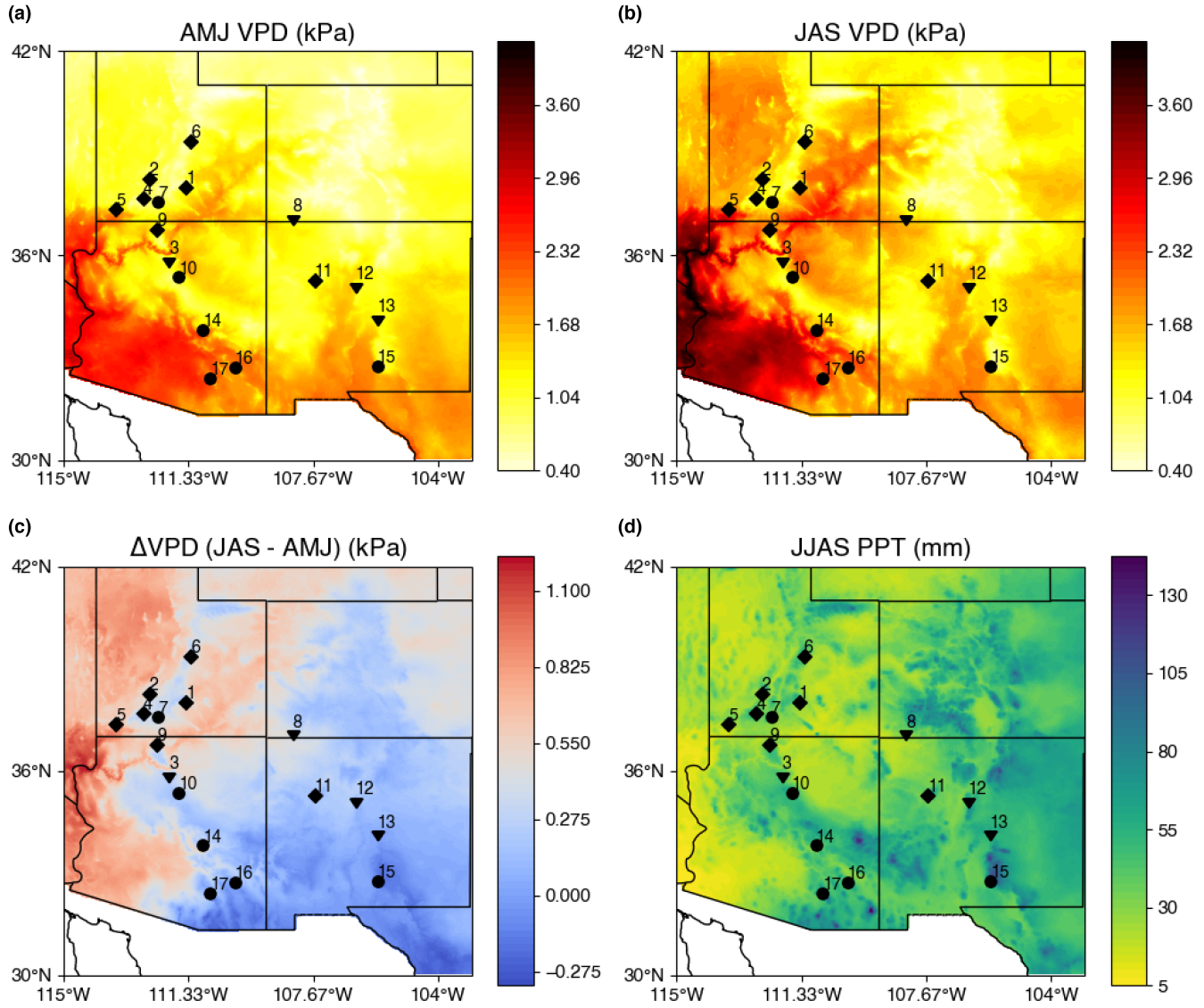

FIGURE 1 (a) Illustrates spring vapor pressure deficit (April, May, and June VPD). (b) Illustrates summer vapor pressure deficit (July, August, and September VPD). (c) The difference between summer and spring vapor pressure deficit (ΔVPD), illustrating the influence of the North American Monsoon on changes in vapor pressure deficit in the SWUS. (d) Illustrates the spatiotemporal patterns of the North American Monsoon for the months June, July, August, and September. All plots are derived from averages from 1960 to 2017. Clusters are denoted by shapes with circles representing NAM-core, diamonds representing NAM-periphery(a), and triangles representing NAM-periphery(b). Corresponding site numbers and site metadata can be found in Table S12.

respective sections (EW1, EW2, and LW) were pooled for all trees at a site to allow for a site-level representation for each section for each respective year. At 10-year intervals, the ring from each individual tree at a site was analyzed separately to assess the within-site variability. In this study, we focused on LW ring widths and carbon isotope ratios ($\delta^{13}C$) because this is the portion of the annual tree ring that most reflects NAM activity (Meko & Baisan, 2001; Szejner et al., 2016). However, EW1 and EW2 observations were also analyzed to remove seasonal covariance effects between EW and LW (Szejner et al., 2018).

On each annual ring, we extracted the α-cellulose from each of the three sub-annual sections following the Soxhlet method detailed in (Leavitt & Danzer, 1993), with the addition of a sodium hydroxide step as detailed in Szejner et al. (2016). The α-cellulose samples were then analyzed for carbon isotopic ratios ($\delta^{13}C$) at the Stable Isotope Ratio Facility for Environmental Research at the University of Utah or at the Environmental Isotope Laboratory of the Department of Geosciences at the University of Arizona. The ratios of $^{13}C/^{12}C$ were measured for the CO_2 produced during α-cellulose combustion using EA-IRMS. Internal reference materials were two glutamic acids with different carbon isotope ratios, calibrated against the USGS40 and USGS41 glutamic acid standards. Values are expressed in the delta (δ) notation relative to the $\delta^{13}C$ Vienna Peedee Belemnite (‰). The $\delta^{13}C$ measurement precision estimated from quality control standards was <0.2‰.

2.3 | Removing early-season influence on LW isotope chronologies

As previous studies have shown that cross-correlations between EW and LW carbon isotopes exist in chronologies from this region (Szejner et al., 2018), we statistically removed any early-season influence on our LW isotope chronologies, producing an independent isotope chronology (referred to as LW adjusted or LW_{adj}). We modified the linear regression method from (Meko & Baisan, 2001) in line with (Szejner et al., 2018) to accomplish this. We first averaged EW1 and EW2 values to estimate total EW $\delta^{13}C$ (which covers the spring and early-summer growth period), then linearly regressed EW against LW carbon isotope chronologies, and finally calculated a residual chronology for each site (subtracting the predicted value from the measured value). As we were calculating WUE, we performed the additional step of adding the mean LW carbon isotope value back to the residuals, yielding our final LW_{adj} chronologies. This ensures that LW_{adj} values are scaled to the original $\delta^{13}C$ time series and suitable for calculating both WUE metrics. The LW_{adj} chronologies were used for all subsequent analyses. Examples of how the LW_{adj} chronologies are calculated can be found in Figure S1. We used three illustrative examples to demonstrate how the correction strength varied depending on the relationship between EW $\delta^{13}C$ and LW $\delta^{13}C$, that is, the correction is larger at sites where there is a strong relationship between EW $\delta^{13}C$ and LW $\delta^{13}C$ and smaller at sites where the relationship is weaker.

2.4 | Calculating WUE_i and WUE_E

To estimate intrinsic and evaporative water-use efficiency, we first calculated the isotopic discrimination (Δ, ‰) for each chronology using the linear model from (Farquhar et al., 1989), including the step of dividing the $\delta^{13}C$ of the sample by 1000 in the denominator.

$$\Delta = \frac{\delta\text{source} - \delta\text{sample}}{1 + \delta\text{sample} / 1000} \quad (1)$$

where δ_{source} is the $\delta^{13}C$ of atmospheric CO_2 and δ_{sample} is the $\delta^{13}C$ of α-cellulose from the tree ring. Following our calculation of isotopic discrimination, we estimated the intercellular concentration of carbon dioxide (c_i; Farquhar et al., 1982).

$$c_i = \left(\frac{\Delta - a}{\bar{b} - a}\right) c_a \quad (2)$$

where Δ is the isotopic discrimination of the sample, a the fractionation associated with CO_2 diffusion (4.4‰), $\bar{b}$ the mean fractionation associated with Rubisco carboxylation when derived from leaf gas-exchange observations (25.5‰), and c_a (ppm) is the atmospheric CO_2 concentration. The $\bar{b}$ term we use, 25.5‰, is drawn from a recent study that proposed an update from the previous value of 27‰ by Cernusak and Ubierna (2022). Although the updated value is drawn from whole wood and we use α-cellulose, we believe it to be a better approximation of the Rubisco fractionation factor than the previous estimate of 27‰. We provide a sensitivity analysis illustrating the discrepancies in WUEi, between the two $\bar{b}$ fractionation factors in Figure S2.

Using estimated c_i, we calculated intrinsic water-use efficiency (WUE_i, Figure 2), the ratio of assimilation/stomatal conductance using the following equation:

$$WUE_i = \frac{A}{g_s} = \frac{g_{CO_2}(c_a - c_i)}{g_{H_2O}} = \frac{c_a - c_i}{1.6} \quad (3)$$

where A is the carbon assimilation, g_s the stomatal conductance, g_{CO_2} the stomatal conductance to CO_2, g_{CO_2} the stomatal conductance to H_2O, and 1.6 is the ratio of diffusivities of water vapor and CO_2. In addition to calculating WUE_i, we calculated evaporative water-use efficiency (WUE_E, Figure 2), reflecting the ratio of assimilation/transpiration using the following equation:

$$WUE_E = \frac{A}{E} = \frac{g_{CO_2}(c_a - c_i)}{g_{H_2O}(e_i - e_a)} = \frac{(c_a - c_i)}{1.6\ \text{vpd}} \quad (4)$$

where E is the transpiration rate, e_i the density ($kg\,m^{-3}$) of water vapor inside the leaf, e_a the density ($kg\,m^{-3}$) of water vapor in the atmosphere, and e_i–e_a the local VPD between the saturated leaf and unsaturated atmosphere. One important distinction between our calculations of WUE_i and WUE_E is that units of c_a, c_i, e_i, e_a, and VPD in WUE_E were converted to a density ($kg\,m^{-3}$) to allow for the ratio of A/E to be accurately represented.

2.5 | Climate data

Precipitation, dew point temperature, and ambient air temperature were downloaded from the PRISM climate data explorer (https://www.prism.oregonstate.edu/explorer/). Calculations for atmospheric VPD from dew point temperature and ambient air temperature were based on derivations from (Buck, 1981). To use the estimated atmospheric VPD as an analog of the local leaf-to-air VPD, in Equation (4), we assumed that needle temperature and atmospheric temperature are equal and that the air temperature derived from the PRISM database is equal to that within tree crowns. We note that Ponderosa pine stands have relatively open canopies and that pine needles are well-coupled to air temperature through efficient convective heat exchange (Schäfer et al., 2010). For seasonal averages of VPD, we used monthly averages of VPD derived from PRISM and then calculated the mean across the months in the window (e.g., JJAS). For seasonal precipitation, we summed the precipitation estimates for each month in the window and calculated the accumulated precipitation across that window (e.g., ONDJFM).

2.6 | Hierarchical clustering and mixed effects modeling

To identify dominant modes of WUE_i variability across our 17 sites, we used an agglomerative hierarchical clustering approach, using the Ward error sum of squares hierarchical clustering method

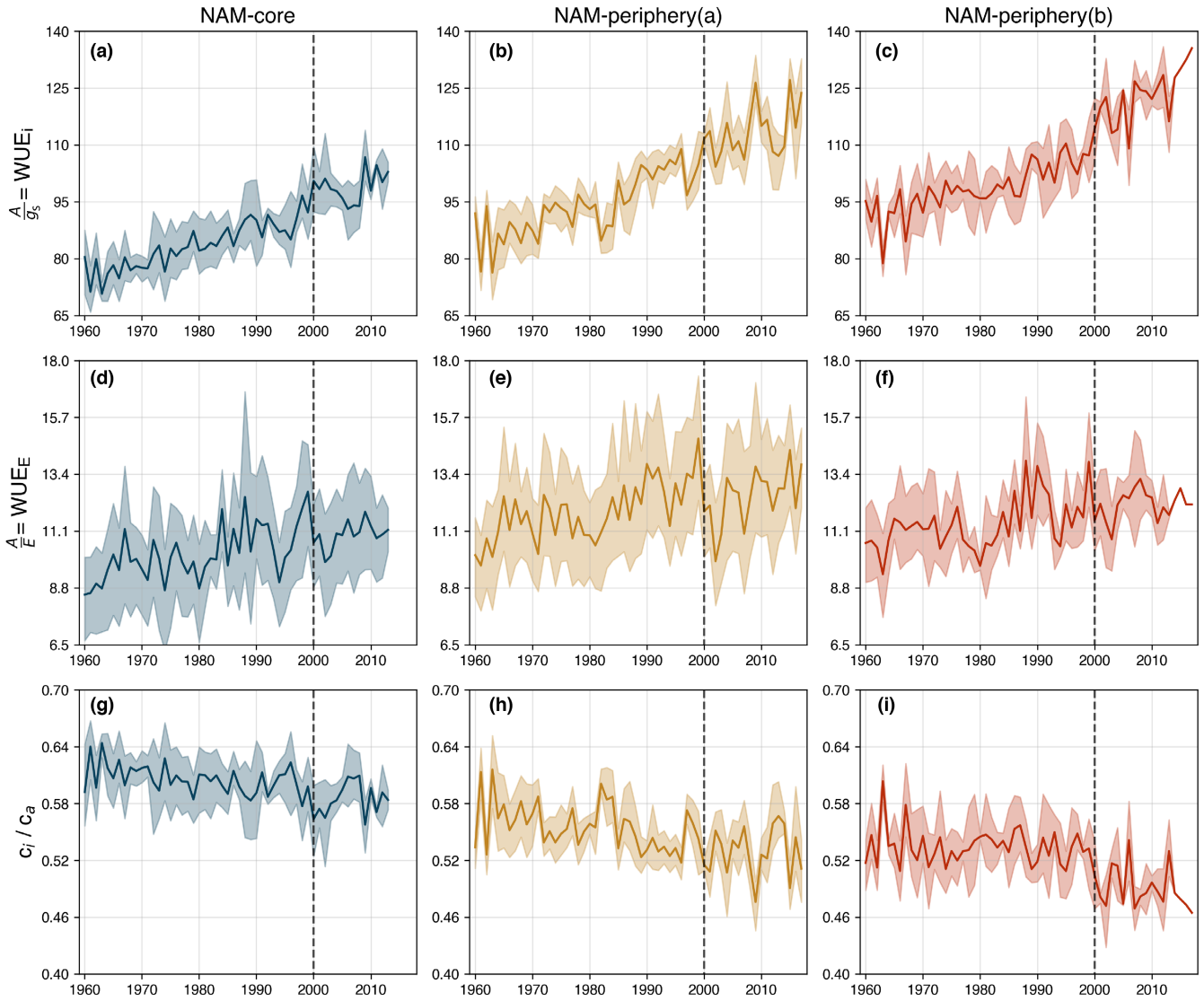

FIGURE 2 Summaries of WUE$_i$ (Assimilation [*A*]/stomatal conductance [g_s]), WUE$_E$ (*A*/transpiration [*E*]), and the ratio of intercellular to atmospheric CO_2 concentrations (c_i/c_a) for NAM-core (a, d, g), NAM-periphery(a) (b, e, h), and NAM-periphery(b) (c, f, i). Solid lines represent means from all sites and shaded regions represent the range from the 10th to 90th percentiles for all sites per year. Vertical dashed lines show the onset of the MD.

(Ward, 1963). This method was used as it does not require a specified number of groups to fit the data to, but rather identifies a number of maximally similar groups based on the chosen characteristic, which in this case was WUE$_i$. By iteratively identifying the most similar WUE$_i$ time series until only one group (all the time series) remains, this approach allowed us to determine the which sites were most similar in terms of physiology and to what degree (Figure S3). This analysis was computationally performed using the SciPy package (Virtanen et al., 2020) in the Python programming language.

To determine the influence of climate and environmental variables on WUE$_i$, we used mixed effects linear models for each cluster with WUE$_i$ as the dependent variable; we used c_a, warm-season precipitation (JJAS), cool-season precipitation (ONDJFM), warm-season VPD (JJAS), and interactions between warm-season VPD and precipitation variables as the independent variables and site as a random effect for this modeling. We grouped all the sites within a cluster together to identify general patterns, and then fit the model across the entire period (1960–2017) for each cluster. Significance for each variable in the model was determined via an alpha value of 0.05. Mixed effects linear modeling was carried out using the Statsmodels package (Seabold & Perktold, 2010) in the Python programming language.

2.7 | WUE$_i$, WUE$_E$, and c_a trend residuals

To assess the potential for increasing VPD to force higher E, independent of decreases in g_s, we examined the relationship between changes in WUE$_i$ (sensitive to g_s) and changes in WUE$_E$ (sensitive to g_s*VPD). Because each WUE time series showed clear increasing trends that strongly correlated with trends in c_a (Figure 2), we first needed to remove the increasing c_a trend, to isolate climate and

environmental influences on WUE. To do so, we calculated the residuals by linearly regressing each WUE metric (WUE_i and WUE_E) time series from 1960 to 2017 with c_a and subtracting the actual values of WUE from the predicted values of WUE. We stress that although we remove the trend of increasing c_a from the WUE time series, the impact of c_a is still present in some capacity on plant physiology (g_s and E). Thus, our interpretation still invokes the response of these physiological variables to increasing c_a. The use of residuals allowed us to also identify plant physiological responses to climate which would otherwise be obscured by the large increasing trend of c_a. We then regressed the residuals from the two WUE terms against each other to assess the intrinsic (WUE_i through g_s) and extrinsic (WUE_E through VPD) controls on tree responses to the MD.

2.8 | RWI analysis

Ring width measurements for earlywood and LW were made on each core collected prior to isotope processing with the Windendro software. Cross-dated series were then detrended using a 100-year spline to preserve high and medium frequency variability. Site chronologies were then calculated using Tukey's biweight robust mean. All RWI chronologies used in these analyses were created using the dplR package in the R programming language (Bunn, 2008). When comparing RWI across clusters, we averaged the RWI for each year and calculated the 10th and 90th percentiles to illustrate variability among the sites in a cluster for a given year.

3 | RESULTS

3.1 | Dominant responses to the MD among 17 forest sites

Three primary clusters emerged from the agglomerative hierarchical clustering analysis: (1) NAM-core, which exhibited low WUE_i, (2) NAM-periphery(a), which exhibited higher WUE_i, and (3) NAM-periphery(b), which exhibited the highest WUE_i. The differences in WUE_i between the three clusters were apparent throughout the entire time series but diverged to an extreme with the onset of the MD (Figure 2a–c), at which point all forests experienced their sharpest increases in WUE_i (NAM-periphery—21%–24%; NAM-core—19%; $p < .001$) and decreases in c_i/c_a (Table 1, Figure 2).

3.2 | Physiological responses as indicated in the c_i response to increasing c_a

From 1960 to 2017, c_a increased from 316 to 405 ppm and mean c_i (estimated from the cross-season adjusted, LW isotope signal LW_{adj} $\delta^{13}C$) also increased across all clusters (Table S1). The c_i/c_a ratio for the pre-MD and MD periods was relatively stable for NAM-core forests, with a mean of 0.6, although early in the MD (2002) c_i/c_a temporarily decreased (Figure 2). However, forests in the NAM-periphery clusters showed highly variable c_i/c_a values during the pre-MD and MD periods (Figure 2), with significant reductions during the MD, and with the largest reductions occurring in NAM-periphery(b) sites (7.4%, $p < .001$, Table 1).

For the NAM-core cluster, our mixed effects model explained 71% of the variance in WUE_i; WUE_i was influenced by c_a ($p < .001$) and a positive interaction of warm-season precipitation and cool-season precipitation ($p < .05$, Table S2). The model for the NAM-periphery(a) cluster, explained 74% of the variance in WUE_i; WUE_i was influenced by c_a ($p < .001$), cool-season precipitation ($p = .054$), and a negative interaction between warm-season precipitation and warm-season VPD ($p < .001$, Table S3). The NAM-periphery(b) model explained 75% of the variance in WUE_i; WUE_i was influenced by c_a ($p < .001$), cool-season precipitation ($p < .005$), and a positive interaction between cool-season precipitation and warm-season VPD ($p < .005$, Table S4).

The primary difference in climate-WUE_i sensitivity among the three clusters, derived from our mixed effects models, was that NAM-core cluster sites showed no significant *direct* sensitivity to interannual variance in precipitation amount or VPD. Instead, the

TABLE 1 Mean values for both WUE and c_i/c_a by period with % change from pre-MD to MD.

Variable	1960–1999 (pre-MD)	2000–2017 (MD)	% change pre-MD to MD	*p*-value for % change	*t*-statistic for % change
WUE_i-NC ($\mu mol\,mol^{-1}$)	83.32	98.96	18.8	1.96e-12	−9.2
WUE_i-NP(a) ($\mu mol\,mol^{-1}$)	93.89	113.54	20.93	1.3e-12	−9.1
WUE_i-NP(b) ($\mu mol\,mol^{-1}$)	98.33	122.8	24.9	1.09e-18	−13.1
WUE_E- NC ($mmol\,mol^{-1}$)	10.18	10.93	7.37	0.02	−2.5
WUE_E- NP(a) ($mmol\,mol^{-1}$)	11.87	12.48	5.14	0.06	−1.9
WUE_E- NP(b) ($mmol\,mol^{-1}$)	11.37	12.16	6.95	0.00	−3
c_i/c_a-NC	0.61	0.58	−4.9	4.9e-5	4.4
c_i/c_a-NP(a)	0.56	0.53	−5.4	0.0	3.9
c_i/c_a-NP(b)	0.53	0.49	−7.5	1.8e-10	7.8

Note: The abbreviations "NC" and "NP" represent NAM-core and NAM-periphery, respectively.

positive interaction term between warm-season precipitation and cool-season precipitation for the NAM-core cluster indicates that during wet winters, WUE_i is more sensitive to warm-season precipitation. The NAM-periphery sites, however, showed a direct sensitivity to precipitation, though in this case it was cool-season precipitation, not NAM precipitation. For the NAM-periphery(a) cluster sites, the negative interaction term between warm-season precipitation and VPD indicates that years with low warm-season precipitation lead to higher sensitivity to warm-season VPD. Finally, for the NAM-periphery(b) cluster sites, the positive interaction term between cool-season precipitation and warm-season VPD indicates that during years with high cool-season precipitation, WUE_i is more sensitive to warm-season VPD.

We performed additional mixed effects modeling on WUE_E to assess its sensitivity to climate and environmental factors. Sites in the NAM-core and NAM-periphery(a) clusters showed significant sensitivity ($p < .005$) to NAM precipitation, warm-season VPD, c_a, and an interaction between NAM precipitation and warm-season VPD (Tables S3 and S5). NAM-periphery(b) sites exhibited similar sensitivities as the two other clusters but were additionally sensitive to winter precipitation and an interaction between winter precipitation and warm-season VPD ($p < .01$; Table S7). The additional influence of winter precipitation indicates that in these sites which receive the least annual precipitation, winter precipitation dynamics, in addition to NAM precipitation, influence late-season WUE_E. We additionally report correlation coefficients for WUE_E and WUE_i versus climate and c_a for both the pre-MD and MD periods in Tables S8–S10.

We found that the clustering of sites by WUE_i generally correlated with NAM intensity (Figure 1); the NAM-core forests were located at more southerly latitudes, associated with the core of the NAM domain, and the NAM-periphery sites were located at more northerly latitudes at the edge of the NAM domain. However, some sites located in the more southerly latitudes, such as Sites 11, 12, and 13 in Figure 1 (GHP, SPP, and CDT) did not cluster with the NAM-core sites. These sites are in areas where the NAM, on average, does not deliver large amounts of precipitation (Figure 1). All three sites are in mountain ranges that lie just beyond the northeastern bulge of NAM precipitation that pushes into southwestern New Mexico (Figure 1d), which could cause patterns in their WUE_i values to better align with NAM-periphery sites.

3.3 | Climate dynamics

We observed large shifts in the hydroclimate toward drier conditions at all sites during the MD (Figure 3, Table S1). Mean values of warm-season precipitation decreased in all clusters from the pre-MD to MD periods, with NAM-core sites decreasing the most (12% decline), though this decrease was primarily driven by a few exceptionally low precipitation years, for example, 2000–2002. Similarly, we observed decreases in cool-season precipitation in all clusters from the pre-MD to the MD periods, ranging from 6.6% to 25% reductions for NAM-periphery(a) and NAM-core, respectively. Concurrent with decreases in precipitation, we observed increases in warm-season VPD from pre-MD to MD across all clusters with the greatest increase occurring in NAM-periphery(a) sites (14.7%, $p < .001$) and NAM-periphery(b) sites (12.6%, $p < .001$). Summer VPD increased least in the NAM-core sites (7%, $p < .01$, Table S1). Thus, the sites within the core NAM region exhibited the largest decreases in warm-season precipitation but were buffered from the most extreme increases in warm-season VPD.

3.4 | Relationship between WUE_i and WUE_E

By examining the relationship between WUE_E residuals (*x*-axis) and WUE_i residuals (*y*-axis) for two time periods, pre-MD (1960–1999) and MD (2000–2017; Figure 4), we identified three scenarios based on a combination of three metrics: level of statistical significance (*p*-value), variance for the dependent variable that is explained by the independent variable (R^2 value), and skewness in the WUE_E and WUE_i residuals (positive or negative). (1) The first scenario we identified (Scenario I) consists of a shallow and positive relationship between the residuals ($p < .01$, $R^2 > .1$), which indicates more positive anomalies in WUE_E than WUE_i (Figure 4g). In our study, we found that this scenario arose primarily as a result of WUE_E residuals with a positive skew >1 and a mean near 0 (*x*-axis), while the distribution of WUE_i residuals generally adhered to normality (mean near zero and skewness ≤|0.5|, *y*-axis). A greater positive skew in WUE_E indicates that E responds to years with cooler climate and lower VPD; the clustering of WUE_i residuals around 0 indicates that g_s is less responsive to climate. This suggests that high WUE_E occurs under a less responsive or constrained g_s, potentially due to elevated CO_2, which may have muted the sensitivity of WUE_i to climate. The NAM-core cluster during the pre-MD period was the only group to clearly exhibit this relationship ($p < .01$, $R^2 = .22$; Figure 4a, Table S12).

The second scenario (Scenario II) we identified showed no significant correlation between residuals ($p > .01$, $R^2 < .1$, Figure 4h), with normally distributed residuals for both WUE_i and WUE_E (mean near 0 and skewness ≤|0.5|). Normally distributed residuals of each WUE metric with a mean value near 0 indicate that both g_s and *E* had similar sensitivities to climate, and that g_s exerted a primary control over *E*. By inference, this means that the elevated CO_2 effect on g_s was absent or negligible. The NAM-core cluster during the MD period was in this second category (Figure 4d, Table S12).

The third scenario (Scenario III) we identified is similar to Scenario I, where the relationship in the WUE residuals is positive ($p < .01$, $R^2 > .1$), but the difference is that in Scenario III, the slope of the relationship is steeper. A steeper slope indicates more positive residuals in WUE_i (*y*-axis) than in WUE_E (*x*-axis; Figure 4i). This steep slope can be driven by positive WUE_i means, and by differing degrees of negative WUE_E means and skewness. In this third scenario, the steeper relationship between the WUE residuals suggests that high rates of *E* occur under low g_s, or in other words, the high reductions in g_s (therefore high WUE_i) do not achieve concomitant

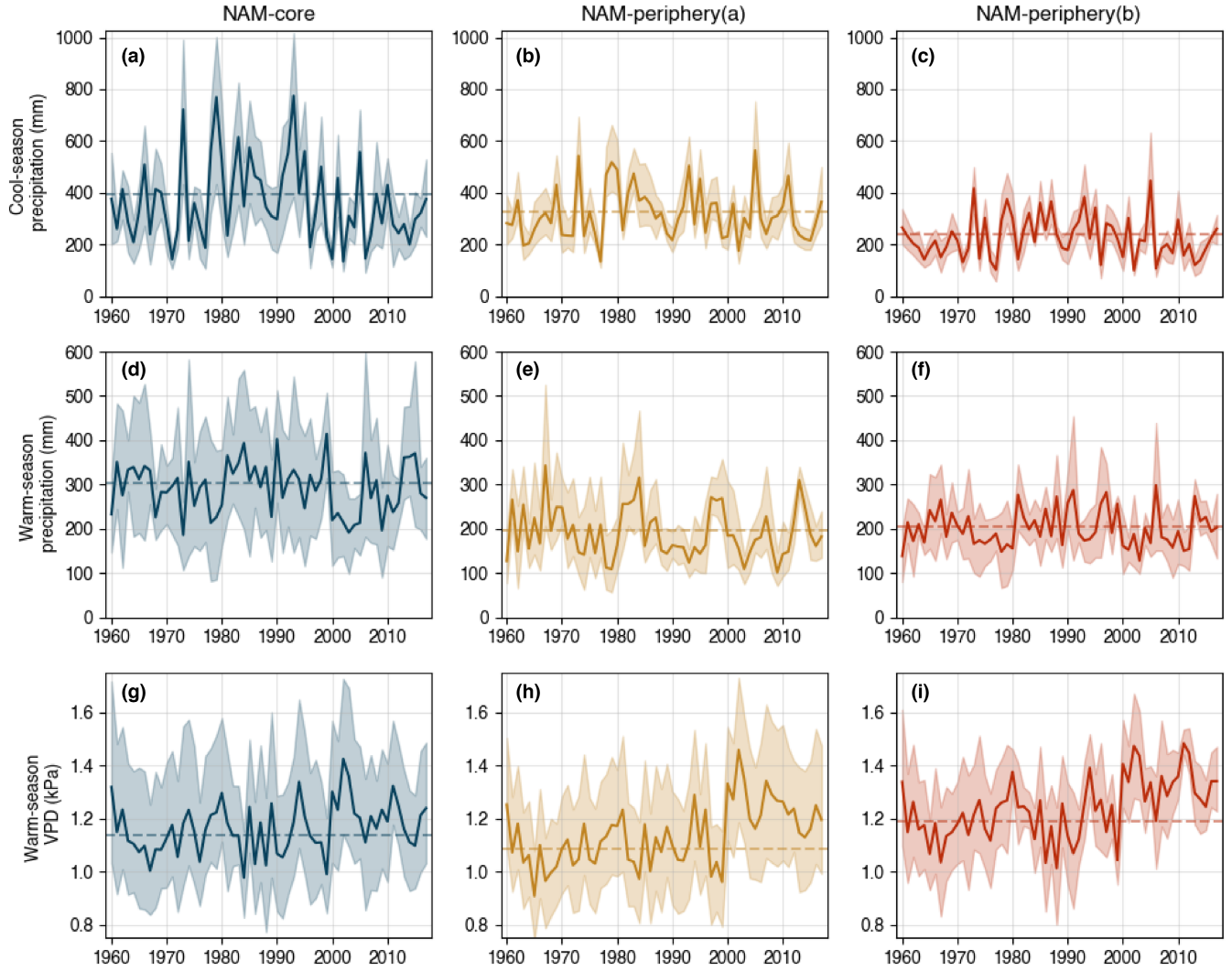

FIGURE 3 Summaries of cool-season precipitation (a–c), monsoon precipitation (d–f), and warm-season vapor pressure deficit (g–i). Clusters are aligned by column with each row representing the aforementioned variables. Shaded regions represent the range between the 10th and 90th percentile for each year while the horizontal dashed lines represent the pre-megadrought mean for each variable.

reductions in E (increases in WUE_E). This implies three things: (1) g_s is not the primary driver of E, (2) VPD is the primary driver of E, and (3) there is no CO_2 enhancement effect. The NAM-periphery(a) and NAM-periphery(b) clusters during the MD fell into this third category (Figure 4e,f).

We suggest that both the NAM-periphery(a) and NAM-periphery(b) clusters during the pre-MD period exist between scenarios I and III, where they exhibited $p < .01$, but the NAM-periphery clusters exhibited lower R^2 values ($R^2 = .17$ for NAM-periphery(a); $R^2 = .16$ for NAM-periphery(b)), indicating a weaker relationship (Figure 4b,c). The slope in the WUE residual relationships for NAM-periphery(a) (slope = 2.28) and NAM-periphery(b) (slope = 2.52) is also not as steep as the slopes of the WUE residual relationships for Scenario III (slope > 4). This implies that these clusters may realize some of the benefits of elevated c_a (Scenario I), but are still experiencing considerable drought stress (Scenario III). See Table S11 for a comprehensive explanation of the three scenarios. We additionally report the mean and skewness of each cluster's WUE_E and WUE_i residuals for each period (pre-MD and MD) in Table S12.

These results show that from pre-MD to MD, the NAM-periphery sites transitioned from residuals having a weak relationship to residuals having a steep, strong relationship. This indicates that as aridity increased during the MD, trees in these clusters experienced higher rates of E (illustrated by reductions in WUE_E residuals), despite reductions in g_s (illustrated by increases in WUE_i residuals). NAM-core sites transitioned from residuals in Scenario I to residuals having no relationship (Scenario II), indicating that the benefits of elevated atmospheric CO_2 diminished during the extremely arid MD and caused an increase in the sensitivity of g_s to climate.

3.5 | Tree growth and WUE relationship

To understand how tree growth responses were influenced in the pre-MD and MD periods, we also examined LW ring width index

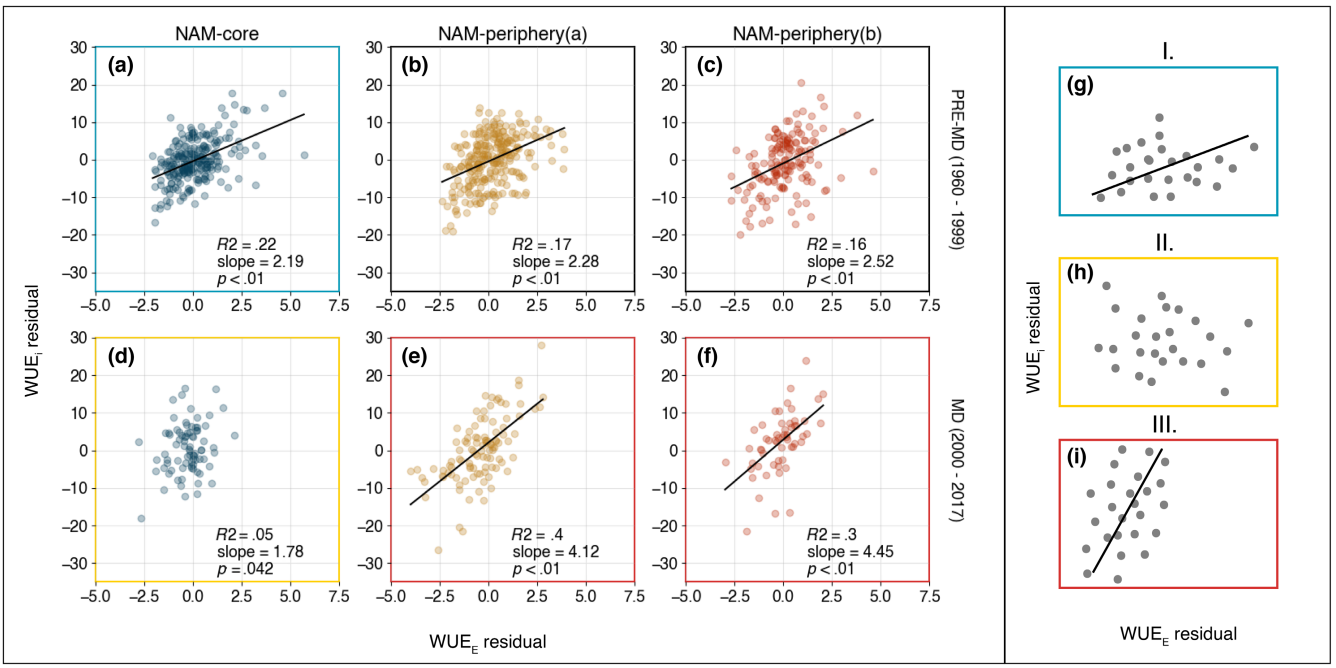

FIGURE 4 Residual plots separated by pre-MD period (a–c) and MD (d–f) for the three clusters. Lines are drawn on plots with a relationship ($R^2 > .1$) with slope denoted in text on the plots. (g) The first scenario (elevated CO_2 reducing stomatal responsiveness), (h) The second scenario (responsive g_s), and (i) The third scenario (decoupled g_s and E). The colored boundaries around panels a–f. correspond to the conceptual diagrams of the three scenarios in panels g–i.

(RWI) across the whole time series (Figure 5). When we compared RWI among the three clusters, we did not find significant differences across the entire time series, although we did find higher RWI variance in the NAM-periphery(b) sites (Figure 5). All three clusters also showed strong reductions in growth in response to the extreme drought of 2002 with the NAM-core, NAM-periphery(a), and NAM-periphery(b) showing a growth reduction of 45%, 66%, and 78%, respectively. Although the drought of 2002 was notable in the RWI of each cluster, it was most distinct in sites falling outside of the NAM domain. Interestingly, while RWI across all clusters appeared to recover following the drought of 2002, WUE_i continued to increase.

4 | DISCUSSION

Our overall findings demonstrate that the MD has affected forests within the core NAM domain differently than forests within the periphery of the NAM domain. We found that during the MD, forests within the core of the NAM domain have been able to limit water loss through inherent physiological adjustments (effective control of E through decreases in g_s), while forests at the fringe of the NAM domain have not (lack of control over E despite decreases in g_s). We were able to make these observations by employing the dual WUE_E and WUE_i approach, which allows the partitioning of physiological and environmental influences on plant water use. We also found that the benefit of past increases in atmospheric CO_2 was not adequate to insulate these forests from enhanced drought stress during the MD, except with the additional benefit of reduced VPD via NAM rains. These conclusions are derived from the residual analysis which showed that NAM-periphery forests exhibited responsive g_s values and NAM-core sites had constrained or less responsive g_s values during the pre-MD period, likely due to elevated c_a reducing the sensitivity of g_s to climate. However, during the MD, NAM-core sites showed g_s becoming more climate sensitive and NAM-periphery sites showed a decoupling of g_s and E, suggesting that the benefit of past increases in c_a did not adequately insulate forests from extreme drought stress. These results demonstrate that if extreme drought conditions continue, the NAM may not be able to continue buffering forests within its domain.

4.1 | WUE_i, WUE_E, and c_i/c_a in a persistent MD

We observed a relatively constant c_i/c_a, ~0.6 and 0.56, for NAM-core and NAM-periphery(a) trees, respectively, which periodically decreased during exceptional drought years, for example, 2002. These results are consistent with optimality theory that interprets c_i/c_a as a homeostatic set point (Ehleringer & Cerling, 1995), which is coordinated by adaptive responses of g_s and A (Voelker et al., 2016). However, trees at the NAM-periphery(b) sites shifted to lower mean c_i/c_a values at the onset of the MD in 2002, which have yet to recover, suggesting an operational shift in the set point during the prolonged aridity of the MD. The long-term implications of this set point change are unclear, but sustained reductions in carbon fixation in the face of

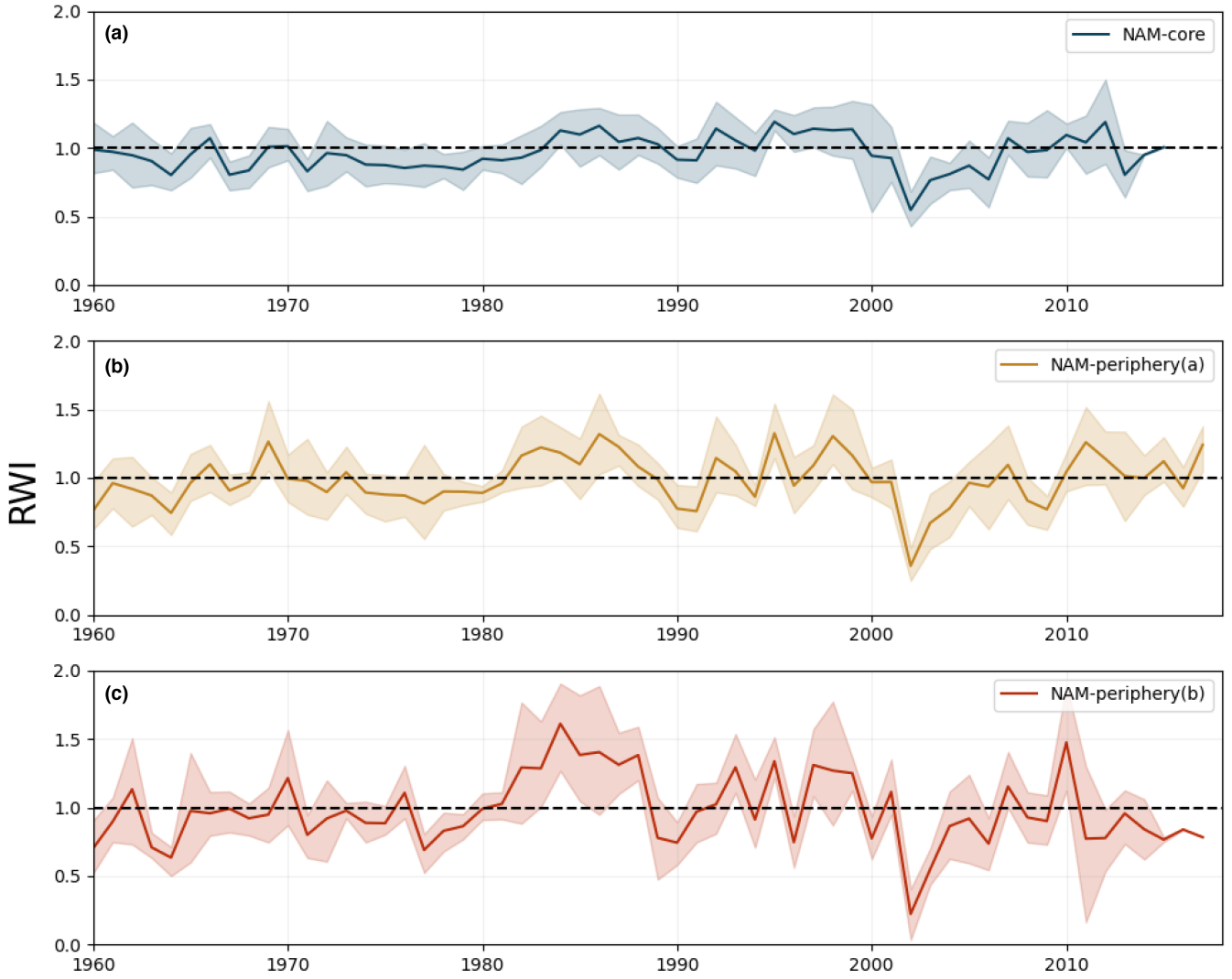

FIGURE 5 Latewood ring width increment (RWI) of the three clusters. Solid lines represent mean RWI for each year across all sites in the cluster. Shaded regions represent the area between the 10th and 90th percentile of RWI for each year across all sites in the cluster. The dashed line represents the mean of the standardized RWI.

lower c_i will potentially reduce the growth of these trees, challenge their ability to defend against herbivores and pathogens, and weaken the carbon sink of the entire SWUS (Piper & Paula, 2020).

Although NAM-periphery trees showed evidence of decreasing g_s and increasing WUE_i during the MD, our findings suggest no additional water savings were achieved through decreases in *E*. These results are consistent with past tree-ring isotope observations that show that despite a 22% increase in WUE_i for European coniferous forests during the 20th century, *E* still increased by 5% (Frank et al., 2015). In general, g_s decreases with increasing temperatures and VPD, thus limiting increases to *E* (Cech et al., 2003; Drake et al., 1997; Leuzinger & Körner, 2007). However, under conditions of sustained drought with high VPD, such as during the warm season at NAM-periphery sites, rates of *E* can remain high, despite low g_s and high WUE_i. Given that WUE_i reflects the ratio of A/g_s and is only a general proxy of water use by plants under ideal situations, the incorporation of WUE_E which accounts for *E* more explicitly is necessary to diagnose the decoupling of g_s and *E* under extreme drought.

An inability to control E, and thus mitigate low WUE_E during persistent drought could be due to inadequate adaptive mechanisms. Coniferous species, including *P. ponderosa*, are known to sustain some significant level of g_s, even during high VPD, rendering needle transpiration rates susceptible to evaporative forces (Monson & Grant, 1989), and more generally, residual transpiration through leaves and needles with relatively closed stomata is common (Boyer et al., 1997; Cochard, 2020; Duursma et al., 2019; Riederer & Schreiber, 2001). It remains to be seen whether a future intensification of the drought, or the long-term effects of the drought to date, impact the fitness of trees in these forests to the point of imposing community shifts in tree phenotypes or even species replacements.

The decoupling of RWI and WUE_i during the MD contrasts with what has been found in other studies (Anderson et al., 1998), where RWI and $\delta^{13}C$ were strongly coupled during drought years. However, the decoupling that we observed is consistent with findings that RWI can be less sensitive to climate than $\delta^{13}C$ (Cernusak & English, 2015; Hartl-Meier et al., 2015). Multiple factors, such as water availability

and VPD interact to influence xylem formation, and for LW formation, carbon availability is also a key factor. The climate influence on $\delta^{13}C$ and WUE_i, however, is expressed through responses in g_s and c_i, which at the leaf level can be highly sensitive to climate. Increasing c_a can also influence WUE_i but may not influence RWI.

From our findings, we propose the use of the dual WUE approach (WUEi vs WUE_E) to provide a more extensive evaluation of forest response to drought, especially in semi-arid and arid landscapes where water is limiting. While WUE_i has its strengths in evaluating plant physiological responses to climate and elevated CO_2 concentrations in more mesic environments or during pluvial periods, elevated VPD in future drought conditions necessitates the use of WUE_E in water-limited ecosystems to account for the role of increased atmospheric aridity on plant water use. The sole reliance on WUE_i to examine forest responses in these semi-arid landscapes to changing climatic conditions may conflate decreased g_s with increased water savings, which we show in this study does not hold true under heightened aridity where a decoupling of g_s and E may occur.

4.2 | The role of increased c_a on drought responses in SWUS forests

Recently, studies have demonstrated that increased atmospheric CO_2 can limit the impacts of increased drought conditions on forests as ambient air temperatures rise (Kirschbaum & McMillan, 2018; Norby & Zak, 2011). Increases in atmospheric CO_2 concentrations reduce g_s, which then reduces E, and this can lead to critical water savings under drought conditions (Sellers et al., 1996; Swann et al., 2016). Our results, however, suggest that any beneficial effect of c_a on E is mitigated during a drought as extreme as the current MD. In our observations, as VPD increased in conjunction with c_a, g_s did indeed decrease, but the role of increased VPD appeared to supersede any benefit of elevated c_a as heightened evaporative demand drove increased E and reduced WUE_E.

The one case in our study in which c_a had a buffering effect on WUE_i and WUE_E was for trees in the NAM-core sites during the pre-MD period (Figure 4a). We hypothesize that mitigation of high summertime VPD by the NAM during the pre-MD period, in conjunction with increasing c_a, led to decreases in g_s and water savings for these sites. However, we saw limited or no evidence of the CO_2 effect for any of the other clusters during the pre-MD or MD period. Again, our approach of incorporating WUE_E in addition to WUE_i allowed us to make this observation, where the sole use of either WUE metric would not have allowed us this insight.

4.3 | Will the NAM continue to buffer forests against extreme drought stress?

It is clear from our study that the impacts of the extreme 20th century MD in the SWUS have been experienced differently across regional forests. In the geographic domain of the NAM climate system, these summer rains have provided a "silver lining" in an otherwise challenging landscape. Warm-season NAM moisture appears to have buffered forests within the core of the NAM domain from the risk of long-term desiccation during the ongoing MD. Conversely, forests on the periphery of the NAM region experienced greater physiological stress during the MD, and more importantly appear to be incapable of mitigating the stress through inherent physiological adjustments.

Whether the buffering nature of the NAM continues to hold as the MD proceeds is uncertain—the NAM is a highly stochastic climate feature and difficult to describe in climate model projections (Cook & Seager, 2013; Meyer & Jin, 2017; Pascale et al., 2017). Shorter duration of NAM rains, or complete failure of the NAM, in a continuing MD would contribute to higher warm-season VPD and diminish the buffering effect that it has on NAM-core sites. Additionally, our analysis illustrates that the once buffered NAM-core forests have more recently transitioned from a favorable drought response (Figure 4g) to a less favorable drought response (Figure 4h), while NAM-periphery forests transitioned from a less favorable drought response to an inadequate drought response (Figure 4i). We hypothesize that the NAM-core forests are on the same trajectory as the NAM-periphery, but they are lagged by one step in the sequence. It remains to be seen if NAM-core forests will progress to the final scenario (desiccation and decoupling of g_s and E; Figure 4i), but increased drought frequency, intensity, and duration will likely drive these forests further along this trajectory.

ACKNOWLEDGMENTS

We thank the two anonymous reviewers whose comments and suggestions helped improve and clarify this manuscript. This work was supported by the Macrosystems program in the Emerging Frontiers section of the U.S. National Science Foundation (NSF award 1065790) and the Ecosystems Program in the Division of Environmental Biology (NSF Award 1754430). BMS, JH, and RKM conceived the research idea. JE oversaw the generation of the stable isotope datasets. BMS performed the data analyses and wrote the initial draft. BMS, RKM, PS, JE, and JH edited subsequent drafts of the manuscript. The tree-ring data and isotope chronologies will be archived in the International TreeRing Databank or will be made available upon request to Brandon Strange (bstrange@ arizona.edu).

CONFLICT OF INTEREST STATEMENT

The authors declare no competing interests.

DATA AVAILABILITY STATEMENT

The data that support the findings of this study will be made openly available NOAA International Tree Ring Data Bank at https://www.ncei.noaa.gov/products/paleoclimatology/tree-ring.

ORCID

Brandon M. Strange https://orcid.org/0000-0003-4236-9271

REFERENCES

Adams, M. A., Buckley, T. N., & Turnbull, T. L. (2020). Diminishing CO_2-driven gains in water-use efficiency of global forests. *Nature Climate Change*, *10*(5), Article 5. https://doi.org/10.1038/s41558-020-0747-7

Ainsworth, E. A., & Rogers, A. (2007). The response of photosynthesis and stomatal conductance to rising [CO_2]: Mechanisms and environmental interactions. *Plant, Cell & Environment*, *30*(3), 258–270. https://doi.org/10.1111/j.1365-3040.2007.01641.x

Allen, C. D., Macalady, A. K., Chenchouni, H., Bachelet, D., McDowell, N., Vennetier, M., Kitzberger, T., Rigling, A., Breshears, D. D., Hogg, E. H. (. T.)., Gonzalez, P., Fensham, R., Zhang, Z., Castro, J., Demidova, N., Lim, J.-H., Allard, G., Running, S. W., Semerci, A., & Cobb, N. (2010). A global overview of drought and heat-induced tree mortality reveals emerging climate change risks for forests. *Forest Ecology and Management*, *259*(4), 660–684. https://doi.org/10.1016/j.foreco.2009.09.001

Anderson, W. T., Bernasconi, S. M., McKenzie, J. A., & Saurer, M. (1998). Oxygen and carbon isotopic record of climatic variability in tree ring cellulose (*Picea abies*): An example from Central Switzerland (1913–1995). *Journal of Geophysical Research: Atmospheres*, *103*(D24), 31625–31636. https://doi.org/10.1029/1998JD200040

Andreu-Hayles, L., Planells, O., Gutiérrez, E., Muntan, E., Helle, G., Anchukaitis, K. J., & Schleser, G. H. (2011). Long tree-ring chronologies reveal 20th century increases in water-use efficiency but no enhancement of tree growth at five Iberian pine forests. *Global Change Biology*, *17*(6), 2095–2112. https://doi.org/10.1111/j.1365-2486.2010.02373.x

Boyer, J. S., Wong, S. C., & Farquhar, G. D. (1997). CO_2 and water vapor exchange across leaf cuticle (epidermis) at various water potentials. *Plant Physiology*, *114*(1), 185–191. https://doi.org/10.1104/pp.114.1.185

Breshears, D. D., Cobb, N. S., Rich, P. M., Price, K. P., Allen, C. D., Balice, R. G., Romme, W. H., Kastens, J. H., Floyd, M. L., Belnap, J., Anderson, J. J., Myers, O. B., & Meyer, C. W. (2005). Regional vegetation die-off in response to global-change-type drought. *Proceedings of the National Academy of Sciences of the United States of America*, *102*(42), 15144–15148. https://doi.org/10.1073/pnas.0505734102

Buck, A. L. (1981). New equations for computing vapor pressure and enhancement factor. *Journal of Applied Meteorology and Climatology*, *20*(12), 1527–1532. https://doi.org/10.1175/1520-0450(1981)020<1527:NEFCVP>2.0.CO;2

Bunn, A. G. (2008). A dendrochronology program library in R (dplR). *Dendrochronologia*, *26*(2), 115–124. https://doi.org/10.1016/j.dendro.2008.01.002

Cech, P. G., Pepin, S., & Körner, C. (2003). Elevated CO_2 reduces sap flux in mature deciduous forest trees. *Oecologia*, *137*(2), 258–268. https://doi.org/10.1007/s00442-003-1348-7

Cernusak, L. A., & English, N. B. (2015). Beyond tree-ring widths: Stable isotopes sharpen the focus on climate responses of temperate forest trees. *Tree Physiology*, *35*(1), 1–3. https://doi.org/10.1093/treephys/tpu115

Cernusak, L. A., & Ubierna, N. (2022). Carbon isotope effects in relation to CO_2 assimilation by tree canopies. In R. T. W. Siegwolf, J. R. Brooks, J. Roden, & M. Saurer (Eds.), *Stable isotopes in tree rings: Inferring physiological, climatic and environmental responses* (pp. 291–310). Springer International. https://doi.org/10.1007/978-3-030-92698-4_9

Cochard, H. (2020). A new mechanism for tree mortality due to drought and heatwaves. *Peer Community In Forest & Wood Sciences*, 1–14. https://doi.org/10.1101/531632

Cook, B. I., & Seager, R. (2013). The response of the North American monsoon to increased greenhouse gas forcing. *Journal of Geophysical Research: Atmospheres*, *118*(4), 1690–1699. https://doi.org/10.1002/jgrd.50111

Drake, B. G., Gonzàlez-Meler, M. A., & Long, S. P. (1997). More efficient plants: A consequence of rising atmospheric CO_2? *Annual Review of Plant Physiology and Plant Molecular Biology*, *48*(1), 609–639. https://doi.org/10.1146/annurev.arplant.48.1.609

Duursma, R. A., Blackman, C. J., Lopéz, R., Martin-StPaul, N. K., Cochard, H., & Medlyn, B. E. (2019). On the minimum leaf conductance: Its role in models of plant water use, and ecological and environmental controls. *New Phytologist*, *221*(2), 693–705. https://doi.org/10.1111/nph.15395

Ehleringer, J. R., & Cerling, T. E. (1995). Atmospheric CO2 and the ratio of intercellular to ambient CO_2 concentrations in plants. *Tree Physiology*, *15*(2), 105–111. https://doi.org/10.1093/treephys/15.2.105

Farquhar, G. D., Ehleringer, J. R., & Hubick, K. T. (1989). Carbon isotope discrimination and photosynthesis. *Annual Review of Plant Physiology and Plant Molecular Biology*, *40*(1), 503–537. https://doi.org/10.1146/annurev.pp.40.060189.002443

Farquhar, G. D., & Richards, R. A. (1984). Isotopic composition of plant carbon correlates with water-use efficiency of wheat genotypes. *Functional Plant Biology*, *11*(6), 539–552. https://doi.org/10.1071/pp9840539

Farquhar, G., O'Leary, M., & Berry, J. (1982). On the relationship between carbon isotope discrimination and the intercellular carbon dioxide concentration in leaves. *Functional Plant Biology*, *9*(2), 121. https://doi.org/10.1071/PP9820121

Francey, R. J., & Farquhar, G. D. (1982). An explanation of 13C/12C variations in tree rings. *Nature*, *297*(5861), 28–31. https://doi.org/10.1038/297028a0

Frank, D. C., Poulter, B., Saurer, M., Esper, J., Huntingford, C., Helle, G., Treydte, K., Zimmermann, N. E., Schleser, G. H., Ahlström, A., Ciais, P., Friedlingstein, P., Levis, S., Lomas, M., Sitch, S., Viovy, N., Andreu-Hayles, L., Bednarz, Z., Berninger, F., … Weigl, M. (2015). Water-use efficiency and transpiration across European forests during the Anthropocene. *Nature Climate Change*, *5*(6), Article 6, 579–583. https://doi.org/10.1038/nclimate2614

Franks, P. J., Adams, M. A., Amthor, J. S., Barbour, M. M., Berry, J. A., Ellsworth, D. S., Farquhar, G. D., Ghannoum, O., Lloyd, J., McDowell, N., Norby, R. J., Tissue, D. T., & von Caemmerer, S. (2013). Sensitivity of plants to changing atmospheric CO_2 concentration: From the geological past to the next century. *New Phytologist*, *197*(4), 1077–1094. https://doi.org/10.1111/nph.12104

Ganey, J. L., & Vojta, S. C. (2011). Tree mortality in drought-stressed mixed-conifer and ponderosa pine forests, Arizona, USA. *Forest Ecology and Management*, *261*(1), 162–168. https://doi.org/10.1016/j.foreco.2010.09.048

Griffin, D., Woodhouse, C. A., Meko, D. M., Stahle, D. W., Faulstich, H. L., Carrillo, C., Touchan, R., Castro, C. L., & Leavitt, S. W. (2013). North American monsoon precipitation reconstructed from tree-ring latewood. *Geophysical Research Letters*, *40*(5), 954–958. https://doi.org/10.1002/grl.50184

Grossiord, C., Buckley, T. N., Cernusak, L. A., Novick, K. A., Poulter, B., Siegwolf, R. T. W., Sperry, J. S., & McDowell, N. G. (2020). Plant responses to rising vapor pressure deficit. *New Phytologist*, *226*(6), 1550–1566. https://doi.org/10.1111/nph.16485

Guerrieri, R., Belmecheri, S., Ollinger, S. V., Asbjornsen, H., Jennings, K., Xiao, J., Stocker, B. D., Martin, M., Hollinger, D. Y., Bracho-Garrillo, R., Clark, K., Dore, S., Kolb, T., Munger, J. W., Novick, K., & Richardson, A. D. (2019). Disentangling the role of photosynthesis and stomatal conductance on rising forest water-use efficiency. *Proceedings of the National Academy of Sciences of the United States of America*, *116*(34), 16909–16914. https://doi.org/10.1073/pnas.1905912116

Hartl-Meier, C., Zang, C., Buntgen, U., Esper, J., Rothe, A., Gottlein, A., Dirnbock, T., & Treydte, K. (2015). Uniform climate sensitivity in tree-ring stable isotopes across species and sites in a mid-latitude temperate forest. *Tree Physiology*, *35*(1), 4–15. https://doi.org/10.1093/treephys/tpu096

Holmes, R. (1983). Computer-assisted quality control in tree-ring dating and measurement. Undefined. https://www.semanticscholar.org/paper/Computer-Assisted-Quality-Control-in-Tree-Ring-and-Holmes/b704f137a9f2a4c87efdf7b16da018c62561cc2f

Kannenberg, S. A., Driscoll, A. W., Szejner, P., Anderegg, W. R. L., & Ehleringer, J. R. (2021). Rapid increases in shrubland and forest intrinsic water-use efficiency during an ongoing megadrought. *Proceedings of the National Academy of Sciences of the United States of America*, *118*(52), e2118052118. https://doi.org/10.1073/pnas.2118052118

Kerhoulas, L. P., Kolb, T. E., & Koch, G. W. (2017). The influence of monsoon climate on latewood growth of southwestern ponderosa pine. *Forests*, *8*(5), 1–16. https://doi.org/10.3390/f8050140

Kirschbaum, M. U. F., & McMillan, A. M. S. (2018). Warming and elevated CO_2 have opposing influences on transpiration. Which is more important? *Current Forestry Reports*, *4*(2), 51–71. https://doi.org/10.1007/s40725-018-0073-8

Lavergne, A., Graven, H., Kauwe, M. G. D., Keenan, T. F., Medlyn, B. E., & Prentice, I. C. (2019). Observed and modelled historical trends in the water-use efficiency of plants and ecosystems. *Global Change Biology*, *25*(7), 2242–2257. https://doi.org/10.1111/gcb.14634

Leavitt, S. W., & Danzer, S. R. (1993). Method for batch processing small wood samples to holocellulose for stable-carbon isotope analysis. *Analytical Chemistry*, *65*(1), 87–89. https://doi.org/10.1021/ac00049a017

Leuzinger, S., & Körner, C. (2007). Water savings in mature deciduous forest trees under elevated CO_2. *Global Change Biology*, *13*(12), 2498–2508. https://doi.org/10.1111/j.1365-2486.2007.01467.x

Mathias, J. M., & Thomas, R. B. (2021). Global tree intrinsic water use efficiency is enhanced by increased atmospheric CO_2 and modulated by climate and plant functional types. *Proceedings of the National Academy of Sciences of the United States of America*, *118*(7), 1–9. https://doi.org/10.1073/pnas.2014286118

Meko, D. M., & Baisan, C. H. (2001). Pilot study of latewood-width of conifers as an indicator of variability of summer rainfall in the North American monsoon region. *International Journal of Climatology*, *21*(6), 697–708. https://doi.org/10.1002/joc.646

Meyer, J. D. D., & Jin, J. (2017). The response of future projections of the north American monsoon when combining dynamical downscaling and bias correction of CCSM4 output. *Climate Dynamics*, *49*(1), 433–447. https://doi.org/10.1007/s00382-016-3352-8

Monson, R. K., & Grant, M. C. (1989). Experimental studies of ponderosa pine. III. Differences in photosynthesis, stomatal conductance, and water-use efficiency between two genetic lines. *American Journal of Botany*, *76*(7), 1041–1047. https://doi.org/10.1002/j.1537-2197.1989.tb15085.x

Mote, P. W., Li, S., Lettenmaier, D. P., Xiao, M., & Engel, R. (2018). Dramatic declines in snowpack in the western US. *Npj Climate and Atmospheric Science*, *1*(1), 1–6. https://doi.org/10.1038/s41612-018-0012-1

Musselman, K. N., Addor, N., Vano, J. A., & Molotch, N. P. (2021). Winter melt trends portend widespread declines in snow water resources. *Nature Climate Change*, *11*(5), 418–424. https://doi.org/10.1038/s41558-021-01014-9

Norby, R. J., & Zak, D. R. (2011). Ecological lessons from free-air CO_2 enrichment (FACE) experiments. *Annual Review of Ecology, Evolution, and Systematics*, *42*(1), 181–203. https://doi.org/10.1146/annurev-ecolsys-102209-144647

O'Donnell, F. C., Donager, J., Sankey, T., Masek Lopez, S., & Springer, A. E. (2021). Vegetation structure controls on snow and soil moisture in restored ponderosa pine forests. *Hydrological Processes*, *35*(11), e14432. https://doi.org/10.1002/hyp.14432

Pascale, S., Boos, W. R., Bordoni, S., Delworth, T. L., Kapnick, S. B., Murakami, H., Vecchi, G. A., & Zhang, W. (2017). Weakening of the North American monsoon with global warming. *Nature Climate Change*, *7*(11), Article 11–Article 812. https://doi.org/10.1038/nclimate3412

Peltier, D. M. P., & Ogle, K. (2019). Legacies of La Niña: North American monsoon can rescue trees from winter drought. *Global Change Biology*, *25*(1), 121–133. https://doi.org/10.1111/gcb.14487

Piper, F. I., & Paula, S. (2020). The role of nonstructural carbohydrates storage in forest resilience under climate change. *Current Forestry Reports*, *6*(1), 1–13. https://doi.org/10.1007/s40725-019-00109-z

Riederer, M., & Schreiber, L. (2001). Protecting against water loss: Analysis of the barrier properties of plant cuticles. *Journal of Experimental Botany*, *52*(363), 2023–2032. https://doi.org/10.1093/jexbot/52.363.2023

Saurer, M., Siegwolf, R. T. W., & Schweingruber, F. H. (2004). Carbon isotope discrimination indicates improving water-use efficiency of trees in northern Eurasia over the last 100 years. *Global Change Biology*, *10*(12), 2109–2120. https://doi.org/10.1111/j.1365-2486.2004.00869.x

Schäfer, K. V. R., Clark, K. L., Skowronski, N., & Hamerlynck, E. P. (2010). Impact of insect defoliation on forest carbon balance as assessed with a canopy assimilation model. *Global Change Biology*, *16*(2), 546–560. https://doi.org/10.1111/j.1365-2486.2009.02037.x

Schimel, D., Kittel, T., Running, S., Monson, R., Turnipseed, A., & Anderson, D. (2002). Carbon sequestration studied in western U.S. Mountains. *Eos Transactions American Geophysical Union*, *83*, *445*, 449. https://doi.org/10.1029/2002EO000314

Seabold, S., & Perktold, J. (2010). Statsmodels: Econometric and statistical modeling with Python. https://doi.org/10.25080/MAJORA-92BF1922-011

Seibt, U., Rajabi, A., Griffiths, H., & Berry, J. A. (2008). Carbon isotopes and water use efficiency: Sense and sensitivity. *Oecologia*, *155*(3), 441–454. https://doi.org/10.1007/s00442-007-0932-7

Sellers, P. J., Bounoua, L., Collatz, G. J., Randall, D. A., Dazlich, D. A., Los, S. O., Berry, J. A., Fung, I., Tucker, C. J., Field, C. B., & Jensen, T. G. (1996). Comparison of radiative and physiological effects of doubled atmospheric CO_2 on climate. *Science*, *271*, 1402–1406. https://doi.org/10.1126/science.271.5254.1402

Sheppard, P. R., Comrie, A. C., Packin, G. D., Angersbach, K., & Hughes, M. K. (2002). The climate of the US southwest. *Climate Research*, *21*(3), 219–238. https://doi.org/10.3354/cr021219

Swann, A. L. S., Hoffman, F. M., Koven, C. D., & Randerson, J. T. (2016). Plant responses to increasing CO_2 reduce estimates of climate impacts on drought severity. *Proceedings of the National Academy of Sciences of the United States of America*, *113*(36), 10019–10024. https://doi.org/10.1073/pnas.1604581113

Szejner, P., Belmecheri, S., Babst, F., Wright, W. E., Frank, D. C., Hu, J., & Monson, R. K. (2021). Stable isotopes of tree rings reveal seasonal-to-decadal patterns during the emergence of a megadrought in the southwestern US. *Oecologia*, *197*, 1079–1094. https://doi.org/10.1007/s00442-021-04916-9

Szejner, P., Belmecheri, S., Ehleringer, J. R., & Monson, R. K. (2020). Recent increases in drought frequency cause observed multi-year drought legacies in the tree rings of semi-arid forests. *Oecologia*, *192*(1), 241–259. https://doi.org/10.1007/s00442-019-04550-6

Szejner, P., Wright, W. E., Babst, F., Belmecheri, S., Trouet, V., Leavitt, S. W., Ehleringer, J. R., & Monson, R. K. (2016). Latitudinal gradients in tree ring stable carbon and oxygen isotopes reveal differential climate influences of the North American Monsoon System. *Journal of Geophysical Research: Biogeosciences*, *121*(7), 1978–1991. https://doi.org/10.1002/2016JG003460

Szejner, P., Wright, W. E., Belmecheri, S., Meko, D., Leavitt, S. W., Ehleringer, J. R., & Monson, R. K. (2018). Disentangling seasonal and interannual legacies from inferred patterns of forest water and carbon cycling using tree-ring stable isotopes. *Global Change Biology*, *24*(11), 5332–5347. https://doi.org/10.1111/gcb.14395

Virtanen, P., Gommers, R., Oliphant, T. E., Haberland, M., Reddy, T., Cournapeau, D., Burovski, E., Peterson, P., Weckesser, W., Bright,

J., van der Walt, S. J., Brett, M., Wilson, J., Millman, K. J., Mayorov, N., Nelson, A. R. J., Jones, E., Kern, R., Larson, E., … van Mulbregt, P. (2020). SciPy 1.0: Fundamental algorithms for scientific computing in Python. *Nature Methods*, *17*(3), 261–272, Article 3. https://doi.org/10.1038/s41592-019-0686-2

Voelker, S. L., Brooks, J. R., Meinzer, F. C., Anderson, R., Bader, M. K.-F., Battipaglia, G., Becklin, K. M., Beerling, D., Bert, D., Betancourt, J. L., Dawson, T. E., Domec, J.-C., Guyette, R. P., Körner, C., Leavitt, S. W., Linder, S., Marshall, J. D., Mildner, M., Ogée, J., … Wingate, L. (2016). A dynamic leaf gas-exchange strategy is conserved in woody plants under changing ambient CO_2: Evidence from carbon isotope discrimination in paleo and CO_2 enrichment studies. *Global Change Biology*, *22*(2), 889–902. https://doi.org/10.1111/gcb.13102

Ward, J. H. (1963). Hierarchical grouping to optimize an objective function. *Journal of the American Statistical Association*, *58*(301), 236–244. https://doi.org/10.1080/01621459.1963.10500845

Williams, A., Allen, C., Macalady, A., Griffin, D., Woodhouse, C., Meko, D., Swetnam, T., Rauscher, S., Seager, R., Grissino-Mayer, H., Dean, J., Cook, E., Gangodagamage, C., Cai, M., & McDowell, N. (2013). Temperature as a potent driver of regional forest drought stress and tree mortality. *Nature Climate Change*, *3*, 292–297. https://doi.org/10.1038/NCLIMATE1693

Williams, A. P., Cook, B. I., & Smerdon, J. E. (2022). Rapid intensification of the emerging southwestern North American megadrought in 2020–2021. *Nature Climate Change*, *12*, 232–234. https://doi.org/10.1038/s41558-022-01290-z

Williams, A. P., Cook, E. R., Smerdon, J. E., Cook, B. I., Abatzoglou, J. T., Bolles, K., Baek, S. H., Badger, A. M., & Livneh, B. (2020). Large contribution from anthropogenic warming to an emerging North American megadrought. *Science*, *368*(6488), 314–318. https://doi.org/10.1126/science.aaz9600

Yocom, L., Ogle, K., Peltier, D., Szejner, P., Liu, Y., & Monson, R. K. (2022). Tree growth sensitivity to climate varies across a seasonal precipitation gradient. *Oecologia*, *198*(4), 933–946. https://doi.org/10.1007/s00442-022-05156-1

SUPPORTING INFORMATION

Additional supporting information can be found online in the Supporting Information section at the end of this article.

How to cite this article: Strange, B. M., Monson, R. K., Szejner, P., Ehleringer, J., & Hu, J. (2023). The North American Monsoon buffers forests against the ongoing megadrought in the Southwestern United States. *Global Change Biology*, *00*, 1–14. https://doi.org/10.1111/gcb.16762